IEEE Conference on Control Applications (CCA)

Cascaded Line-of-Sight Path-Following and Sliding Mode Controllers for Fixed-Wing UAVs

João Fortuna* and Thor I. Fossen†
Centre for Autonomous Marine Operations and Systems (AMOS), Department of Engineering Cybernetics
Norwegian University of Science and Technology, Trondheim, Norway
Email: *joao.fortuna at itk.ntnu.no, †fossen at ieee.org

***Abstract*—This paper describes a nonlinear controller for following references generated by a Line-of-Sight (LOS) guidance algorithm. Good performance is achieved even in disturbed conditions without integral action by controlling the vehicle's course instead of heading. A cascaded system architecture is employed and a uniform semiglobal exponential stability (USGES) proof is presented. Software-in-the-loop simulation results support the theoretical conclusions.**

***Index Terms*—Unmanned aerial vehicle (UAV), guidance systems, sliding mode control, nonlinear control systems**

I. Introduction

Efficient path-following laws are paramount in the development of autonomous unmanned vehicles. In order to achieve accurate path-following suitable for practical applications, such guidance systems must be able to handle environmental disturbances. For Unmanned Aerial Vehicles (UAVs) the main source of disturbances is wind.

When tackling the problem of path-following for autonomous vehicles, lookahead-based steering guidance laws such as LOS provide good performance at a lower computational cost than other approaches, as discussed in [1] and [2]. Small UAVs are particularly affected by varying wind. To minimize the error caused by the wind during path-following, the usual approach involves using an integral term in the guidance algorithm. In this paper we will explore an alternative concept that relies on controlling the course of the aircraft instead of the heading. Because there is no integrator that needs time to intensify its effect, course control should achieve better performance.

Sliding mode is a type of robust control that allows for model uncertainties. This family of controllers reduces n^{th}-order systems to a simpler first-order system which is easier to control. In its most simple form, the sliding control output switches between positive and negative values in a discontinuous manner at high frequency when close to the equilibrium point, this is referred to as chattering. In [3] the issue of undesired excitation of unmodelled high-frequency modes by chattering is discussed. The solution presented suggests a trade-off between accuracy and modelling complexity by using continuous saturation functions instead of discontinuous switches. The authors of [4] opt for using the smoother $\tanh$ function instead of the signum function.

This work was supported by the Norwegian Research Council (grant no. 223254) through the Centre of Autonomous Marine Operations and Systems (AMOS) at the Norwegian University of Science and Technology.

This paper builds on results obtained for marine vehicles in [5] and [6], and applies it to aircraft dynamics. In Section II we will describe the proposed problem and aircraft kinematic model. Section III will explore the LOS and sliding mode algorithms. Following that, in Section IV we discuss simulation results and implementation details. Finally, Section V presents some remarks and concluding comments.

II. Problem Formulation

Since in most common operation of small UAVs the required paths are straight lines connecting waypoints, that will be the case explored in this paper. In order to simplify notation and calculations, the Path State block in Figure 1 continuously converts the vehicle state from the inertial frame to the path frame. The path reference system has its origin in the starting waypoint, the x-axis is pointing in the direction of the target waypoint and the z-axis is pointing downwards, see Figure 2. For the sake of less cluttered notation we will also drop the p subscript for variables in the path frame.

When a waypoint is reached and the next one is loaded, the origin of the path frame is updated. Due to this coordinate change, the y-coordinate of the vehicle in the path frame will be the cross-track error.

A. Model

If we consider a constant altitude flight, the bank-to-turn regime applies and the kinematic model can be written as in [7]:

$$\dot{x} = V_a \cos(\psi) + W_x = V_g \cos(\chi) \tag{1a}$$

$$\dot{y} = V_a \sin(\psi) + W_y = V_g \sin(\chi) \tag{1b}$$

$$\dot{\psi} = \frac{g}{V_a} \tan(\varphi) \tag{1c}$$

$$\dot{\varphi} = -\frac{\varphi - \varphi_{\text{cmd}}}{T_\varphi} \tag{1d}$$

$$W = \sqrt{W_x^2 + W_y^2} \tag{1e}$$

The variable pair (x, y) represents the position of the UAV, ψ is the heading and χ is the course of the aircraft, φ is the

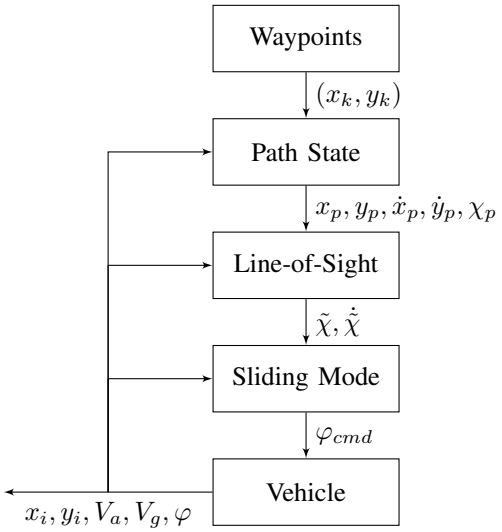

Fig. 1. Cascaded System

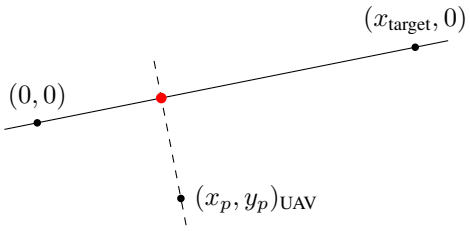

Fig. 2. Path reference frame

roll angle while φ_{cmd} is the commanded roll that is sent to the Autopilot. The control input is φ_{cmd}.
V_a is the forward scalar airspeed in body-frame, V_g is the scalar ground speed and g is the gravitational acceleration.
Equation (1d) from [8] captures the dynamics of the change in roll which is not instantaneous, T_φ represents the time constant of the roll variation, the lower it is the faster the UAV will reach the commanded roll. In practice, it decreases the oscillations in control. W is the total average wind, which is the norm of the average wind in the x and y-directions.

To avoid the kinematic singularity in the model, we approximate (1c) by:

$$\dot{\psi} = \frac{g}{V_a}\frac{\sin(\varphi)}{\varepsilon(\varphi)} \tag{2a}$$

$$\varepsilon(\varphi) = \begin{cases} \cos(\varphi) & \text{, if } \ |\cos(\varphi)| \geq \varepsilon' \\ \varepsilon' & \text{, if } \ 0 \leq \cos(\varphi) < \varepsilon' \\ -\varepsilon' & \text{, if } \ -\varepsilon' < \cos(\varphi) < 0 \end{cases} \tag{2b}$$

$$\ddot{\psi} \approx \frac{g}{V_a}\dot{\varphi}\frac{1}{\varepsilon^2(\varphi)} \tag{2c}$$

where ε' is a small positive constant. An alternative to avoid the singularity could be to use unit quaternions.
To avoid the need for integral action in the presence of wind, we will control the UAV by course instead of heading angle. The course rate is given by (3) while acceleration is given in Appendix A.

$$\chi = \tan^{-1}\left(\frac{\dot{y}}{\dot{x}}\right) \tag{3a}$$

$$\dot{\chi} = \frac{\dot{x}\ddot{y} - \dot{y}\ddot{x}}{\dot{x}^2 + \dot{y}^2} \tag{3b}$$

$$= \frac{(V_a\cos(\psi) + W_x)\left(V_a\dot{\psi}\cos(\psi)\right)}{V_g^2} + \frac{(V_a\sin(\psi) + W_y)\left(V_a\dot{\psi}\sin(\psi)\right)}{V_g^2} \tag{3c}$$

$$= \dot{\psi}\frac{V_a^2 + V_a\left(\cos(\psi)W_x + \sin(\psi)W_y\right)}{V_g^2} \tag{3d}$$

$$= \frac{g\sin(\varphi)\left(V_a + \cos(\psi)W_x + \sin(\psi)W_y\right)}{\varepsilon(\varphi)V_g^2} \tag{3e}$$

III. Tools and Methods

To achieve the proposed goal of path-following under influence of wind-induced disturbances we will employ a cascaded system architecture. This structure is shown in Figure 1.

The Path State block will feed cross-track error and course data to the LOS algorithm. After generating the desired course and course rate, the LOS subsystem feeds the current error to the Sliding Mode controller. The last step will be to output a desired roll command that is sent to the vehicle's low level autopilot.

A. Line-of-Sight Guidance

A LOS guidance law is given by (4) in a similar approach to the one in [6]. Although, because of the coordinate change and the restriction to straight paths, the path angle variable can be excluded. The resulting guidance law is written as:

$$\chi_d = \tan^{-1}\left(-\frac{y}{\Delta}\right) \tag{4a}$$

$$\dot{\chi}_d = -\frac{\Delta}{\Delta^2 + y^2}\dot{y} \tag{4b}$$

$$\ddot{\chi}_d = \frac{\Delta}{\left(\Delta^2 + y^2\right)^2}\left(2y\dot{y}^2 - \left(\Delta^2 + y^2\right)\ddot{y}\right) \tag{4c}$$

where Δ is a lookahead distance, and χ_d and $\dot{\chi}_d$ are respectively desired course and desired course rate. y is the cross-track error, and due to the frame change is also the y-coordinate of the UAV.
Theorem 1 in [6] proves USGES of the equilibrium point $y = 0$.

Having arrived at expressions for the dynamics of the desired course, we can then define $\tilde{\chi}$ as the course error:

$$\tilde{\chi} = \chi - \chi_d \tag{5}$$

If we combine (1b), (4a) and (5) we get

$$\dot{y} = V_g\sin\left(\tilde{\chi} + \tan^{-1}\left(-\frac{y}{\Delta}\right)\right) \tag{6}$$

which is equivalent to

$$\dot{y} = V_g \sin(\tilde{\chi}) \cos\left(\tan^{-1}\left(-\frac{y}{\Delta}\right)\right) + V_g \cos(\tilde{\chi}) \sin\left(\tan^{-1}\left(-\frac{y}{\Delta}\right)\right) \quad (7)$$

and can be further reduced to

$$\dot{y} = V_g \sin(\tilde{\chi}) \frac{\Delta}{\sqrt{\Delta^2 + y^2}} - V_g \cos(\tilde{\chi}) \frac{y}{\sqrt{\Delta^2 + y^2}} \quad (8)$$

This can be written as

$$\dot{y} = -\frac{V_g y}{\sqrt{\Delta^2 + y^2}} + V_g \tau(y, \tilde{\chi}) \tilde{\chi} \quad (9a)$$

$$\tau(y, \tilde{\chi}) = \frac{\sin(\tilde{\chi})}{\tilde{\chi}} \frac{\Delta}{\sqrt{\Delta^2 + y^2}} - \frac{\cos(\tilde{\chi}) - 1}{\tilde{\chi}} \frac{y}{\sqrt{\Delta^2 + y^2}} \quad (9b)$$

B. Sliding Mode Control

In order to drive the course and course rate errors to 0, a sliding surface s is defined as:

$$s = \dot{\tilde{\chi}} + \lambda \tilde{\chi} \quad (10a)$$

$$\dot{s} = \ddot{\tilde{\chi}} + \lambda \dot{\tilde{\chi}} \quad (10b)$$

The error dynamics will be described by:

$$\dot{\tilde{\chi}} = \dot{\chi} - \dot{\chi}_d \quad (11)$$

and

$$\ddot{\tilde{\chi}} = \ddot{\chi} - \ddot{\chi}_d \quad (12a)$$

$$= u + f\left(\tilde{\chi}, \dot{\tilde{\chi}}\right) \quad (12b)$$

$$= \varphi_{\text{cmd}} \frac{g\left(V_a + W_x \cos(\psi) + W_y \sin(\psi)\right)}{V_g^2 T_\varphi \varepsilon^2(\varphi)} + f\left(\tilde{\chi}, \dot{\tilde{\chi}}\right) \quad (12c)$$

where $f\left(\tilde{\chi}, \dot{\tilde{\chi}}\right)$ represents the evolution of $\ddot{\tilde{\chi}}$ when there is no control input, i.e. the nominal system.
Next we use the following Lyapunov candidate function and its derivative:

$$V = \frac{1}{2} s^2 \quad (13a)$$

$$\dot{V} = s\dot{s} \quad (13b)$$

$$= s\left(\ddot{\tilde{\chi}} + \lambda \dot{\tilde{\chi}}\right) \quad (13c)$$

$$= s\left(\lambda \dot{\tilde{\chi}} + u + f\left(\tilde{\chi}, \dot{\tilde{\chi}}\right)\right) \quad (13d)$$

then, if we choose u so that it cancels out the remaining terms of $\dot{s}$:

$$u = -\lambda \dot{\tilde{\chi}} - \rho \text{sgn}(s) - K_d s \quad (14a)$$

$$\dot{V} = s\left(f\left(\tilde{\chi}, \dot{\tilde{\chi}}\right) - \rho \text{sgn}(s) - K_d s\right) \quad (14b)$$

$$= f\left(\tilde{\chi}, \dot{\tilde{\chi}}\right) s - \rho|s| - K_d s^2 \quad (14c)$$

If we set ρ sufficiently large:

$$\rho > \left|f\left(\tilde{\chi}, \dot{\tilde{\chi}}\right)\right| \quad (15)$$

Then we can cancel any effect of the unactuated system, even if we have modelling errors. Moreover:

$$\dot{V} = \underbrace{f\left(\tilde{\chi}, \dot{\tilde{\chi}}\right) s - \rho|s|}_{\leq 0} - K_d s^2 \quad (16a)$$

$$\leq -K_d s^2 \quad (16b)$$

According to Theorem 4.10 in [9] the origin $s = 0$ is globally exponential stable (GES) if K_d is a positive constant.
Now we need to find the bound $f_{\max}$ of $f\left(\tilde{\chi}, \dot{\tilde{\chi}}\right)$ such that ρ in (15) can be specified. Appendix B contains the steps to get to the bound $f_{\max}$. The second expression in Appendix B-(27e) is particularly useful when tuning the controller for a specific UAV and environmental conditions. The bound will depend on the aircraft capabilities when compared to the environment: the larger the difference between the achievable airspeed and wind speed, the lower the bound will be. Next we choose:

$$\rho \geq f_{\max} \quad (17a)$$

$$\varphi_{\text{cmd}} = u \frac{V_g^2 T_\varphi \varepsilon^2(\varphi)}{g\left(V_a + W_x \cos(\psi) + W_y \sin(\psi)\right)} \quad (17b)$$

Where u is given by (14a).

C. Cascaded Stability Analysis

The closed-loop system is a cascade. Following the example in [5]:

$$\Sigma_1 : \dot{y} = f_1(t, y) + g(t, y, \tilde{\chi}) \tilde{\chi} \quad (18a)$$

$$\dot{y} = \underbrace{-\frac{V_g y}{\sqrt{\Delta^2 + y^2}}}_{f_1(t,y)} + \underbrace{V_g \tau(y, \tilde{\chi})}_{g(t,y,\tilde{\chi})} \tilde{\chi} \quad (18b)$$

where τ is given by (9b). The second sub-system is

$$\Sigma_2 : \dot{\tilde{\chi}} = f_2(t, \tilde{\chi}) \quad (19)$$

Lemma 1. *(USGES of Cascaded System) Let χ_d be calculated according to (4a) and φ_{cmd} be obtained with (17b) by computing u through (14a) such that the restrictions in (26) hold. Then the origin of the cascaded system ($s = 0$ and $\tilde{\chi} = 0$) is a uniformly semiglobal exponentially stable (USGES) equilibrium point.*

Proof. The system in (18) is USGES as proven in [6]. GES of system (19) is proven in Section III-B. Property 1 in [5] regarding the boundedness of the interconnecting term applies to this system with the same bound. Hence, all the necessary conditions for USGES of the cascaded system are met according to Proposition 2.3 in [10]. □

IV. Results

The control system was implemented in the DUNE [11] [12] open-source framework and was tested with the Ardupilot [13] software-in-the-loop (SITL) suite, which uses JSBSim [14] to simulate the aircraft dynamics. JSBSim is a highly complex simulator that provides accurate data, which is close to real flight data, including uncertainties such as sensor noise or actuation delays. The simulation architecture

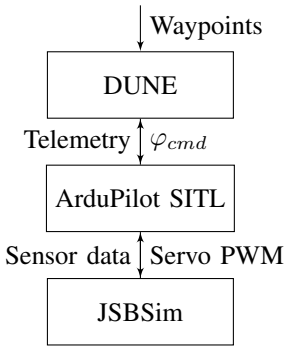

Fig. 3. Simulation architecture.

is shown in Figure 3. Developed code is available online at [15].

We consider a small UAV with the following specifications:

$$V_a = 20 \quad \text{(m/s)} \tag{20a}$$
$$m = 6.6 \quad \text{(kg)} \tag{20b}$$
$$\text{wingspan} = 2.8 \quad \text{(m)} \tag{20c}$$
$$\text{length} = 1.9 \quad \text{(m)} \tag{20d}$$

and the wind conditions to be:

$$W_E \approx 0 \quad \text{(m/s)} \tag{21a}$$
$$W_N \approx 10 \quad \text{(m/s)} \tag{21b}$$

It is important to notice that such conditions would usually be avoided for real flights of said airframe.

Equation (14a) is the most usual way to choose u according to the sliding mode literature. However, to avoid chattering in the practical implementation, u is instead defined using the smooth $\tanh$ function as in [4]:

$$u = -\lambda\dot{\tilde{\chi}} - \rho \tanh\left(\frac{s}{bandwidth}\right) - K_d s \tag{22}$$

The following values were obtained after tuning iteratively in simulation:

$$\Delta = 50 \tag{23a}$$
$$\rho = 4 \tag{23b}$$
$$\lambda = 2 \tag{23c}$$
$$bandwidth = 5 \tag{23d}$$
$$K_d = 3 \tag{23e}$$
$$T_\varphi = 0.1 \tag{23f}$$

Another adjustment made for implementation was to limit $|\varphi_{cmd}|$ to $45\,\text{deg}$. The ρ obtained from tuning is much lower than the predicted in Appendix B, this is due to the need to be very conservative in order to reach global results for the stability proof.

Figure 4 shows results from two simulations. In both cases the desired path was a long line such that the dominant wind direction was parallel to the y-axis in the path reference frame. In the scenario with wind, the oscillations in cross-track error are mostly due to wind gusts that the simulated wind estimator does not react to sufficiently fast.

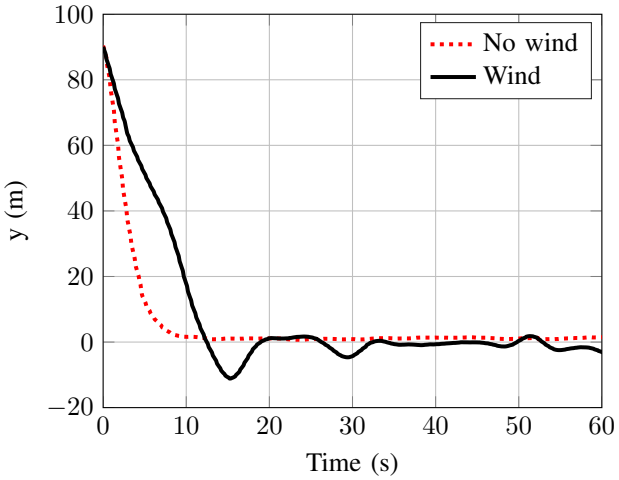

Fig. 4. Cross-track error.

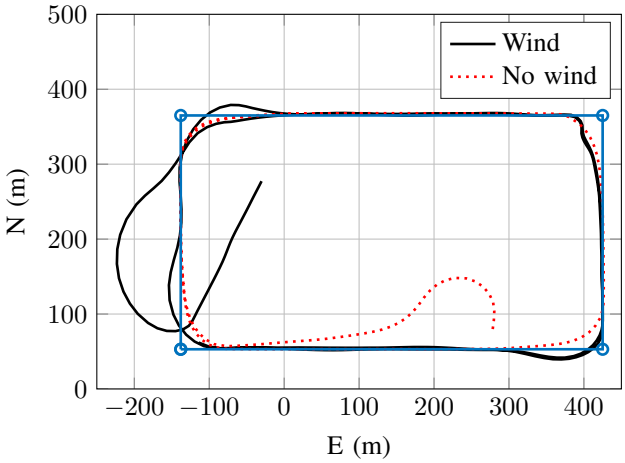

Fig. 5. Rectangular path waypoints and actual path for different wind conditions.

The graph in Figure 5 shows the waypoints and the path followed by the aircraft in two different environmental conditions. Notice that the start conditions are also different for both scenarios, so the performance should only be compared after first passing the North-West waypoint.
After the initial approach phase to each line segment, the cross-track error is virtually unnoticeable in both scenarios. Furthermore, the waypoints are located considerably close to each other. In a real flight mission, the short approach phase would be irrelevant when compared to the total transect.
In Figures 6 and 7 we can see the plots of a small interval of the commanded and actual roll angles for the scenarios without and with wind respectively. The peaks in commanded roll correspond to sharp changes in direction when waypoints change.

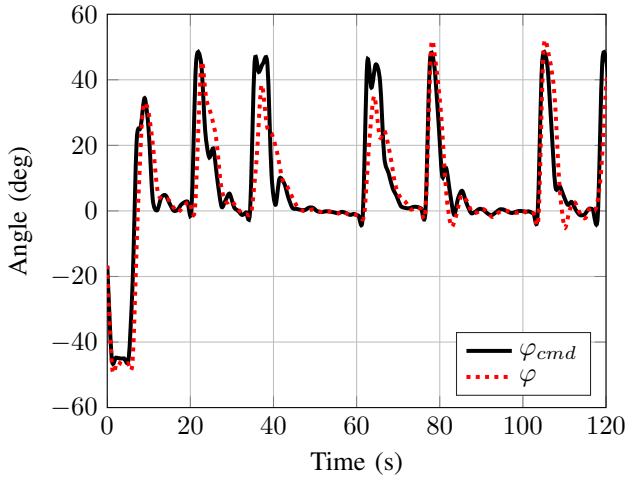

Fig. 6. Roll and commanded roll in no-wind scenario.

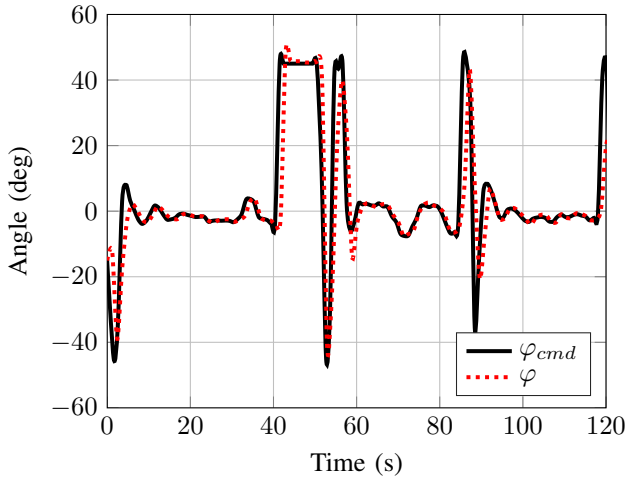

Fig. 7. Roll and commanded roll in wind scenario.

V. Conclusions

This paper presents a uniform semiglobal exponential stability (USGES) proof of a cascaded LOS path-following and sliding mode control system for fixed-wing UAVs. Furthermore, simulation results show a promising performance. Future work includes flight testing the controller.

Appendix A
Course acceleration

Equation (24) gives the course acceleration.

Appendix B
Bound of nominal course acceleration error

Equation (27) gives the bound of $f\left(\tilde{\chi}, \dot{\tilde{\chi}}\right)$.

$$\ddot{\chi}_d = \frac{\Delta}{\left(\Delta^2 + y^2\right)^2}\left(2y\dot{y}^2 - \left(\Delta^2 + y^2\right)\ddot{y}\right) \tag{25a}$$

$$= \frac{\Delta}{\left(\Delta^2 + y^2\right)^2}\Big(2y\left(V_a \sin(\psi) + W_y\right)^2 - \left(\Delta^2 + y^2\right) g \frac{\sin(\varphi)}{\varepsilon(\varphi)} \cos(\psi)\Big) \tag{25b}$$

$$= \frac{\Delta 2y\left(V_a \sin(\psi) + W_y\right)^2}{\left(\Delta^2 + y^2\right)^2} - \frac{\Delta g \sin(\varphi)\cos(\psi)}{\varepsilon(\varphi)\left(\Delta^2 + y^2\right)} \tag{25c}$$

The bounds in (26b)–(26c) are so that in the worst case scenario – flying against the wind – it is still possible to reach the destination.

$$\Delta_{\min} \leq \Delta \leq \Delta_{\max} \tag{26a}$$

$$0 < V_{\min} \leq V_a \tag{26b}$$

$$W = \delta V_a, \quad 0 \geq \delta < 1 \tag{26c}$$

$$T_\varphi > 0 \tag{26d}$$

References

[1] M. Breivik and T. I. Fossen, "Guidance laws for autonomous underwater vehicles. Ch. 4," in *Underwater Vehicles*. IN-TECH, 2009, pp. 51–76.

[2] T. I. Fossen, *Handbook of marine craft hydrodynamics and motion control*. Wiley, 2011.

[3] J.-J. E. Slotine and W. Li, *Applied nonlinear control. Ch. 7*. Prentice Hall New Jersey, 1991.

[4] A. Healey and D. Lienard, "Multivariable sliding mode control for autonomous diving and steering of unmanned underwater vehicles," *IEEE Journal of Oceanic Engineering*, vol. 18, no. 3, pp. 327–339, 1993.

[5] T. I. Fossen and A. M. Lekkas, "Direct and indirect adaptive integral line-of-sight path-following controllers for marine craft exposed to ocean currents," *International Journal of Adaptive Control and Signal Processing*, 2015.

[6] T. I. Fossen and K. Y. Pettersen, "On uniform semiglobal exponential stability (USGES) of proportional line-of-sight guidance laws," *Automatica*, vol. 50, no. 11, pp. 2912–2917, 2014.

[7] R. W. Beard and T. W. McLain, *Small Unmanned Aircraft: Theory and Practice*. Princeton University Press, 2012.

[8] R. Bencatel, "Perpetual flight in flow fields," Porto, Portugal, May 2012.

[9] H. K. Khalil, *Nonlinear systems*. Prentice Hall New Jersey, 2002.

[10] A. Loría and E. Panteley, "Cascaded nonlinear time-varying systems: Analysis and design. Ch. 2," in *Advanced Topics in Control Systems Theory*, ser. Lecture Notes in Control and Information Science. Springer London, 2005, vol. 311, pp. 23–64.

[11] LSTS, "DUNE," https://github.com/LSTS/dune, last accessed in April, 2015.

[12] J. Pinto, P. Dias, R. Martins, J. Fortuna, E. Marques, and J. Sousa, "The LSTS toolchain for networked vehicle systems," in *OCEANS - Bergen, Norway, 2013 MTS/IEEE*, 2013, pp. 1–9.

[13] 3DRobotics, "Ardupilot," http://plane.ardupilot.com, last accessed in April, 2015.

[14] "JSBSim," http://jsbsim.sourceforge.net/, last accessed in April, 2015.

[15] J. Fortuna, "DUNE - SMC," https://github.com/LSTS/dune/blob/4c93f40835a8f96fc71ac1a7886e4ee2825a1f6c/src/Control/Path/SMC/Task.cpp, last accessed in April, 2015.

$$\ddot{\chi} = \frac{y^{(3)}\dot{x} - x^{(3)}\dot{y}}{\dot{x}^2 + \dot{y}^2} + 2\frac{(\dot{y}\ddot{x} - \dot{x}\ddot{y})(\dot{x}\ddot{x} + \dot{y}\ddot{y})}{\left(\dot{x}^2 + \dot{y}^2\right)^2} \tag{24a}$$

$$= \underbrace{\varphi_{\text{cmd}} \frac{g}{V_g^2 T_\varphi \varepsilon^2(\varphi)} \left(V_a + W_x \cos(\psi) + W_y \sin(\psi)\right)}_{u} + \frac{g^2 \sin^2(\varphi)}{V_g^2 V_a \varepsilon^2(\varphi)} \left(W_y \cos(\psi) - W_x \sin(\psi)\right)$$

$$- g\frac{V_g^2\varphi + 2T_\varphi \sin(\varphi)\varepsilon(\varphi)\left(W_y \cos(\psi) - W_x \sin(\psi)\right)}{V_g^4 T_\varphi \varepsilon^2(\varphi)} \left(V_a + W_x \cos(\psi) + W_y \sin(\psi)\right) \tag{24b}$$

$$f_{\max} \geq \left|\ddot{\chi}\right|_{u=0} + \left|\ddot{\chi}_d\right| \tag{27a}$$

$$\geq \left| g\frac{V_g^2\varphi + 2T_\varphi \sin(\varphi)\varepsilon(\varphi)\left(W_y \cos(\psi) - W_x \sin(\psi)\right)}{V_g^4 T_\varphi \varepsilon^2(\varphi)} \left(V_a + W_x \cos(\psi) + W_y \sin(\psi)\right) \right| +$$

$$\left| \frac{\Delta 2y \left(V_a \sin(\psi) + W_y\right)^2}{\left(\Delta^2 + y^2\right)^2} \right| + \left| \frac{\Delta g \sin(\varphi)\cos(\psi)}{\varepsilon(\varphi)\left(\Delta^2 + y^2\right)} \right| + \left| \frac{g^2 \sin^2(\varphi)}{\varepsilon^2(\varphi) V_g^2 V_a} \left(W_y \cos(\psi) - W_x \sin(\psi)\right) \right| \tag{27b}$$

$$= g\frac{{}^{\pi}/_{2} V_g^2 + T_\varphi W}{V_g^4 T_\varphi \varepsilon'^2} \left(V_a + W\right) + 0.65 \left(\frac{V_a + W}{\Delta_{\min}}\right)^2 + \frac{g}{\Delta_{\min}\varepsilon'} + \frac{g^2}{V_g^2 V_a \varepsilon'^2} W \tag{27c}$$

$$= \frac{g}{\varepsilon'^2} \left(\frac{{}^{\pi}/_{2} V_g^2 + T_\varphi W}{V_g^4 T_\varphi} \left(V_a + W\right) + \underbrace{\frac{0.65\varepsilon'^2 \left(V_a + W\right)^2}{g\Delta_{\min}^2}}_{\approx 0} + \underbrace{\frac{\varepsilon'}{\Delta_{\min}}}_{\approx 0} + \frac{gW}{V_g^2 V_a} \right) \tag{27d}$$

$$\approx \frac{g}{\varepsilon'^2} \left(\frac{{}^{\pi}/_{2} V_g^2 + T_\varphi W}{V_g^4 T_\varphi} \left(V_a + W\right) + \frac{gW}{V_g^2 V_a} \right) = \frac{g}{\left(V_a \varepsilon'\right)^2} \left(\frac{{}^{\pi}/_{2} V_a \left(1 - \delta\right)^2 \left(1 + \delta\right) + T_\varphi \left(1 + \delta\right)\delta}{T_\varphi \left(1 - \delta\right)^4} + \frac{g\delta}{\left(1 - \delta\right)^2} \right) \tag{27e}$$